Supplement of Atmos. Chem. Phys., 24, 11045–11061, 2024
https://doi.org/10.5194/acp-24-11045-2024-supplement

Atmospheric Chemistry and Physics
Open Access
EGU

Supplement of

Online characterization of primary and secondary emissions of particulate matter and acidic molecules from a modern fleet of city buses

Liyuan Zhou et al.

Correspondence to: Chak K. Chan (chak.chan@kaust.edu.sa) and Åsa M. Hallquist (asa.hallquist@ivl.se)

Section S1. Mass-to-charge ratio (m/z) calibration.

In this study, six isolated ion peaks (O_2-, CNO-, $C_3H_5O_3$-, $C_2F_3O_3$-, $C_5F_9O_2$-, $C_{10}HF_9O_4$-) were identified as suitable for m/z calibration over the entire studied m/z range. Accuracies are reported as parts-per-million of the m/z value (ppm), calculated as:

$$\text{Accuracy [ppm]} = (m/z_{comp} - m/z_{cal})/(m/z_{cal}) \times 10^6, \quad (1)$$

where m/z_{comp} is the peak position, m/z_{cal} is the calibration value. The average accuracy achieved for all six m/z calibrants was within 3 ppm (Table S1), determined from a weighted average of all m/z calibration accuracies and their standard deviations. The accuracy for ions not used in the m/z calibration is also evaluated. Several overlapping peaks are recorded at most integer m/z, and multi-peak fitting is performed to determine individual signal intensities (Figure S3). This procedure may introduce additional uncertainty in the determined peak positions beyond the m/z accuracy of isolated peaks. To estimate the accuracy for the measured ions, multi-peak fits of peaks with known individual peak positions were performed. Table S2 shows the average biases and m/z accuracies for five (Cl-, NO_2-, NO_3-, $C_3H_5O_3$-, $C_8H_{15}O_2$-) ions, determined from a time series of several hours of individual spectra. The table lists values for both isolated peaks and those in multiple-peak groups. The average accuracies estimated for the isolated peaks are similar to those for the m/z calibration peaks, but larger for the multiple peak cases, reflecting the additional uncertainties due to the proximity of other peaks.

Section S2. Calculation of emission factors (EFs)

The EFs are calculated as the quantity of pollutant emitted per kilogram of fuel combusted, employing the carbon balance method adapted from established methodologies in our prior work and other studies in the field (Ban-Weiss et al., 2009; Hak et al., 2009; Hallquist et al., 2013; Zhou et al., 2020):

$$EF_{pollutant} = \left(\frac{\int_{t_1}^{t_2}([pollutant]_t - [pollutant]_{t_1})dt}{\int_{t_1}^{t_2}([CO_2]_t - [CO_2]_{t_1})dt}\right) \times EF_{CO_2}, \quad (2)$$

where $EF_{pollutant}$ denotes the emission factor for the specific pollutant. The time interval from t_1 to t_2 is critical for capturing the emission dynamics from individual buses. This interval starts just before the sharp rise in pollutant concentration (t_1) and ends as levels stabilize and blend with ambient conditions (t_2), as illustrated in Figure S4, similar to methods we have described previously (Zhou et al., 2020; Zhou et al., 2021). This approach ensures the robustness of peak integration, given that contributions beyond t_2 typically oscillate around zero. The start and end times, t_1 and t_2, for each pollutant peak are independently determined to account for the differing response times of the measuring instruments to the exhaust plume. The resultant concentration changes of the pollutant and CO_2, recorded between t_1 and t_2, are integral to this calculation. For EF_{CO_2}, specific values are assigned based on the type of fuel used, consistent with values reported in earlier studies: 3156 g kg^{-1} for DSL, 2834 g kg^{-1} for RME, 3107 g kg^{-1} for HVO and 2536 g kg^{-1} for CNG (Edwards et al., 2004).

Section S3. OH exposure in Go:PAM.

The OH_{exp} in Go:PAM was calculated using the model described by Watne et al. (2018). Briefly, a chemical model containing a comprehensive description of ozone photolysis and HO_x chemistry and a skeleton description of NO_x, CO, HC and SO_x chemistry was used to mimic the gas-phase chemistry in Go:PAM (Table S3). The minimum OH exposure was derived for each bus passage plume using the maximum NO_x, HC and CO concentrations in Go:PAM and the corresponding water and ozone concentrations. The assumed speciation of HC was aldehydes (26%), alkanes (33%), alkenes (14%) and aromatic compounds (27%). The oxidation capacity of Go:PAM was offline calibrated by SO_2 as described by Lambe et al. (2011), where the photon flux at 254 nm, $P_{FLUX254}$= 1.57×10^{16} cm^{-2} $s^{-1,}$ and first order loss rates of OH were derived by matching the measured and modeled SO_2 and O_3 decreases.

Recently, a concern of non-OH chemistry in the OFR has been raised. (Peng et al., 2016) In this study, we estimated the ratios of exposures of non-OH species to OH exposure for O_3, $O(^1D)$ and $O(^3P)$. The relative importance of non-OH chemistry was evaluated according to Peng et al. (Peng et al., 2016), by taking toluene as a surrogate as it is a common SOA precursor found in vehicle emissions (Gentner et al., 2017; Liu et al., 2019). The undesired VOC destructions by O_3, $O(^1D)$ and $O(^3P)$ were negligible (close to 0 %). The direct photolysis of aromatics in Go:PAM has been evaluated by Watne et al. (2018) under similar experimental conditions (photon flux, residence time). No reductions of toluene and trimethyl-benzene were observed with UV light on.

Section S4. Classification of acetate-CIMS measured species.

The identities of the organic compounds are assigned based on knowledge of the sensitivities of the ionization scheme and the expected compounds emitted from the buses. These compounds were classified into nine families on the basis of their molecular characteristics, according to Liu et al. (2017). Briefly, the functional group composition of ions containing C, H or O atoms was estimated from its elemental composition using the number of oxygen atoms (n_o) and double bound equivalency (DBE, calculated as $1+n_c-1/2n_H$), assuming (1) each ion has at least one carboxylic acid group, (2) the excess oxygen ($n_o - 2$) is contained in hydroxy or keto groups, (3) the excess DBE (DBE − 1) is due to keto groups (priority) or alkene groups, and (4) a phenyl group exists if DBE ≥ 5. The ions are categorized into acid classes using the following prioritized criteria: (1) if DBE ≥ 5, the ion is categorized as an aromatic acid, otherwise (2) if $n_o = 2$, the ion is assigned as a monoacid (either saturated (DBE=1) or unsaturated (DBE>1)), (3) if $n_o > 2$, and $n_o > 2 \times$ DBE, the ion is counted as a hydroxy acid, (4) in the case of $n_o > 2$ and $n_o \leq 2 \times$ DBE (DBE ≥ 2), the ions is defined as a carbonyl acid if n_o is an odd number, otherwise the ion is referred to as a diacid or hydroxycarbonyl acid. For ions containing N or S atoms, (1) if the $n_N > 0$, and $n_S=0$, ions is assigned as a nitrogen (N)-containing compounds (no S), (2) if the $n_S > 0$, and $n_N=0$, ions is assigned as a sulfur (S)-containing compounds (no N), (3) if the $n_N > 0$, and $n_S>0$, ions is assigned as a N and S-containing compounds. Table S4 lists the classification for the ions identified in this study.

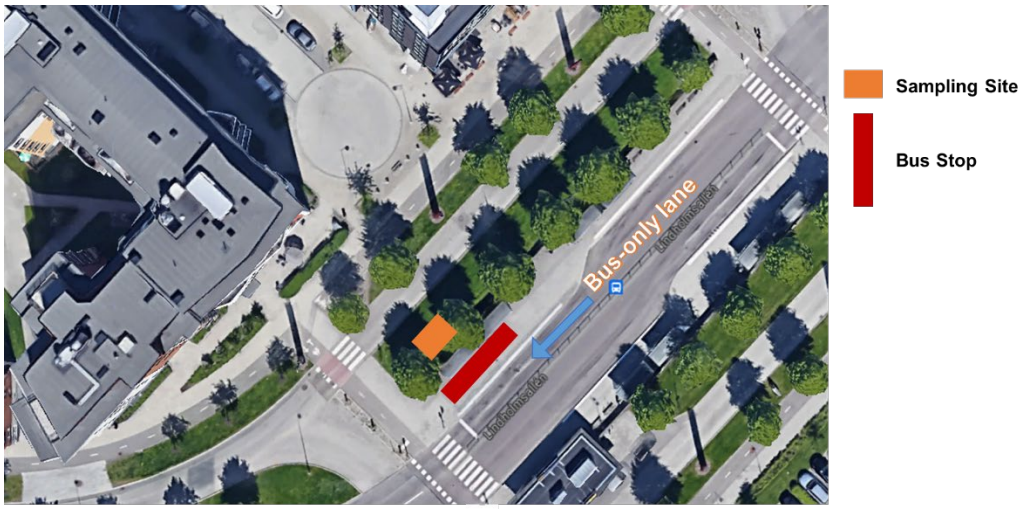

Figure S1. Satellite image of the roadside sampling site at Lindholmen, Gothenburg, Sweden. Map data: © Google, DigitalGlobe.

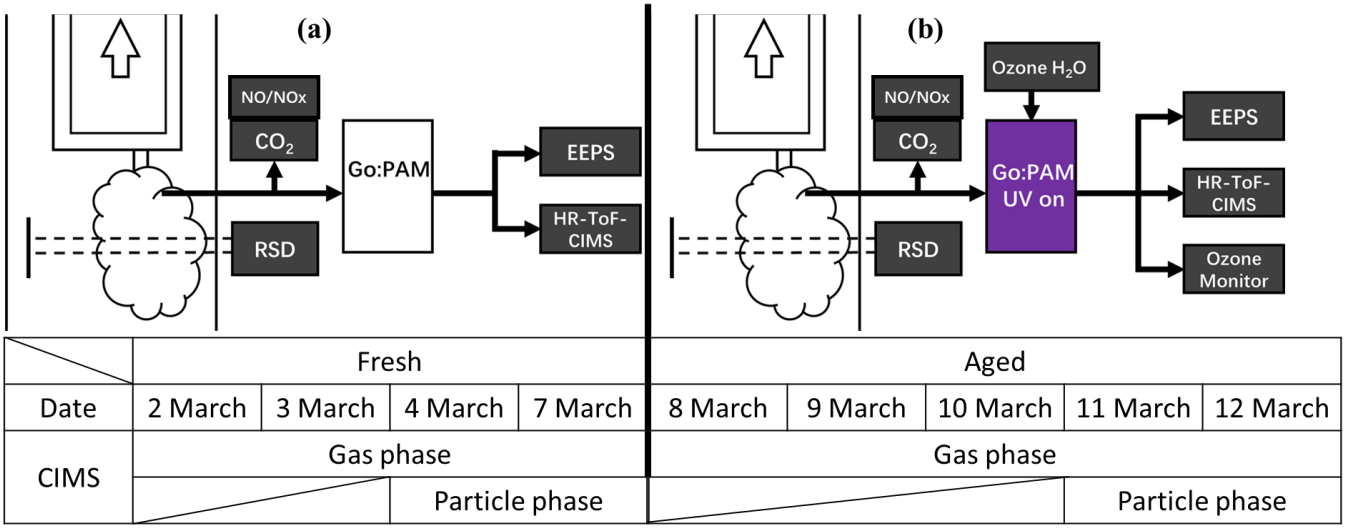

Figure S2. Schematic of the roadside measurement. (a) fresh emission measurements, (b) aged measurements: photo-oxidation of bus plumes. RSD (Remote Sensing Device), CO_2 analyzer, NO/NO_x analyser, EEPS (Engine Exhaust Particle Sizer), and HR-ToF-CIMS (high-resolution time-of-flight chemical-ionization mass spectrometer).

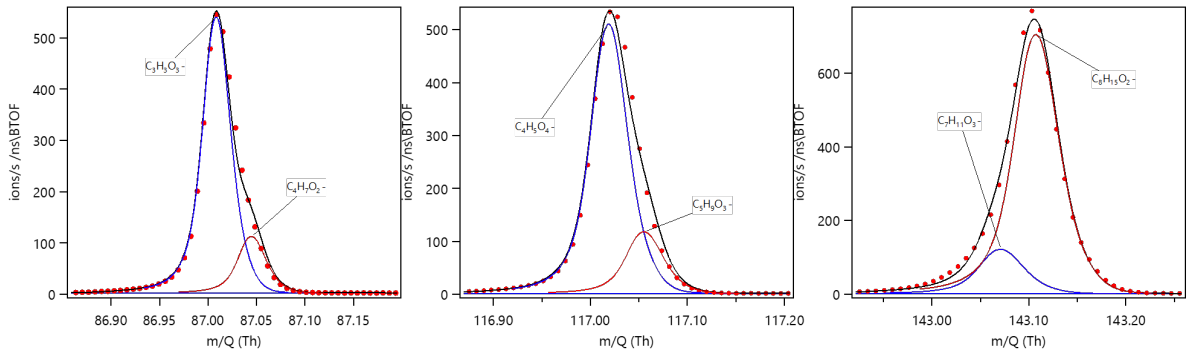

Figure S3. Example peak fits of major ions.

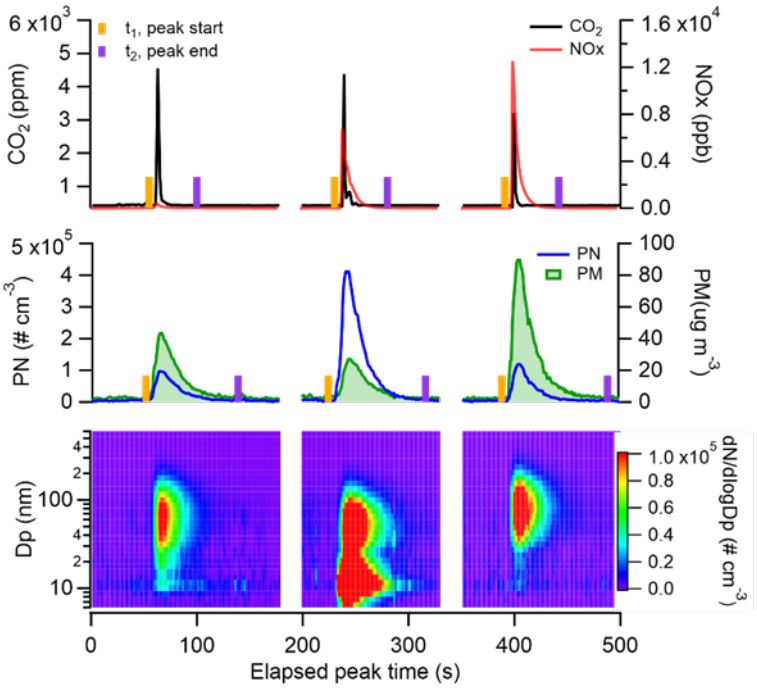

Figure S4. Representative concentration profiles of CO_2, NOx, particle number (PN), particle mass (PM), and particle number size distribution measured from three individual buses.

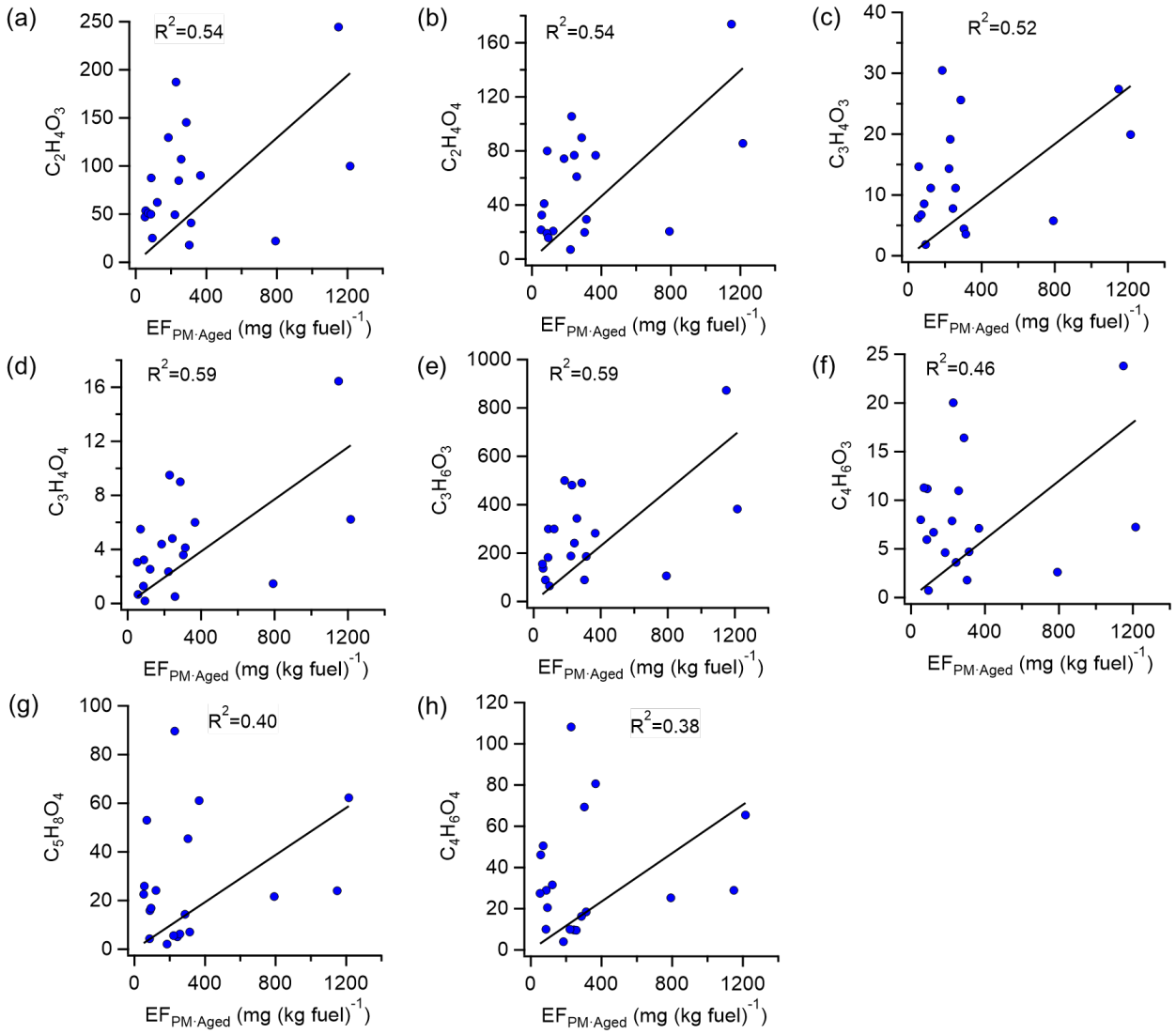

Figure S5. Correlations between ion counts of most abundant gas-phase organic acids and $EF_{PM:aged}$ (a-h) from 19 buses after oxidation in the Go:PAM.

Table S1. Isolated ion peaks for m/z calibration.

Exact, m/z	Assigned formula	Accuracy±1σ (ppm)
31.990378	O_2-	0.2±0.1
41.998537	CNO-	2.6±1.1
89.024418	$C_3H_5O_3$-	2.9±2
112.985587	$C_2F_3O_3$-	3.2±2.7

262.976007	$C_5F_9O_2$-	3.1±1

Table S2. The average biases and m/z accuracies for five ions (determined from a time series of several hours of individual spectra).

Exact, m/z	Assigned formula	Accuracy±1 (ppm)	Comments
34.969401	Cl-	3.7±3.2	Isolate peak
89.024418	$C_3H_5O_3$-	1.5±1.2	Isolate peak
61.988366	NO_3-	1.2±1	Isolate peak
45.993452	NO_2-	2.8±1.2	Isolate peak
143.107753	$C_8H_{15}O_2$-	3.7±5	Multi-peak

Table S3. Reactions and rate coefficients for model calculations of OH exposure. The data were taken from the literature as described in Watne et al. * 74% of measured HC, **26% of measured HC.

No.	Reaction	k (cm^3 $molecule^{-1}$ s^{-1})
1	$O_3+hv \rightarrow O_2+O(^1D)$	0.18
2	$O(^1D)+H_2O \rightarrow OH+OH$	1.99×10^{-10}
3	$O(^1D)+O_2 \rightarrow O(^3p)+O_2$	3.97×10^{-11}
4	$O(^1D)+O_3 \rightarrow O_2+O(^3p)+O(^3p)$	1.2×10^{-10}
5	$O(^1D)+O_3 \rightarrow O_2+O_2$	1.2×10^{-10}
6	$O(^1D)+N_2 \rightarrow O(^3p)+N_2$	3.11×10^{-11}
7	$O(^3p)+O_2+M \rightarrow O_3+M$	6.1×10^{-34}
8	$O(^3p)+O_3 \rightarrow O_2+O_2$	7.96×10^{-15}
9	$O(^3p)+OH \rightarrow H+O_2$	3.29×10^{-11}
10	$H+O_2 \rightarrow HO_2$	9.57×10^{-13}
11	$H+HO_2 \rightarrow OH+OH$	7.2×10^{-11}
12	$H+HO_2 \rightarrow O(^3p)+H_2O$	1.6×10^{-12}
13	$H+HO_2 \rightarrow H_2+O_2$	6.9×10^{-12}
14	$OH+OH \rightarrow H_2O+O(^3p)$	1.8×10^{-12}
15	$OH+OH \rightarrow H_2O_2$	6.29×10^{-12}
16	$OH+O_3 \rightarrow HO_2+O_2$	7.25×10^{-14}
17*	$HO_2+HO_2 \rightarrow H_2O_2+O_2$	3.28×10^{-12}
18**	$HC+OH \rightarrow 0.7RO_2+0.3HO_2$	1.0×10^{-11}
19	$HCHO+OH \rightarrow H_2O+CO+HO_2$	9.2×10^{-12}
20	$SO_2+OH \rightarrow OHSO_2$	9.59×10^{-13}
21	$OHSO_2+O_2 \rightarrow SO_3+HO_2$	4.3×10^{-13}
22	$NO+O(^3p) \rightarrow NO_2$	1.66×10^{-12}
23	$NO_2+hv \rightarrow NO+O(^3p)$	1.64×10^{-4}
24	$NO_2+OH \rightarrow HNO_3$	1.06×10^{-11}
25	$NO_2+OH \rightarrow HOONO$	1.79×10^{-12}
26	$HO_2+NO \rightarrow NO_2+OH$	8.16×10^{-12}

27	$RO_2+NO \rightarrow RO+ NO_2$	9×10^{-12}
28	$O(^1D)+N_2+M \rightarrow N_2O+M$	2.82×10^{-36}
29	$N_2O+O(^1D) \rightarrow N_2+O_2$	5.09×10^{-11}
30	$N_2O+O(^1D) \rightarrow NO+NO$	7.64×10^{-11}
31	$O(^3p)+HO_2 \rightarrow OH+O_2$	5.87×10^{-11}
32	$O(^3p)+ H_2O_2 \rightarrow OH+HO_2$	1.7×10^{-15}
33	$H+O_3 \rightarrow OH+O_2$	2.89×10^{-11}
34	$HO_2+O_3 \rightarrow OH+O_2+O_2$	1.93×10^{-15}
35	$HO_2+ OH \rightarrow H_2O +O_2$	1.11×10^{-10}
36	$H_2O_2+hv \rightarrow OH+OH$	1.05×10^{-3}
37	$HO_2+hv \rightarrow OH+O(^1D)$	4.07×10^{-3}
38	$OH+ H_2O_2 \rightarrow HO_2+H_2O$	1.8×10^{-12}
39	$NO+O_3\rightarrow NO_2+O_2$	1.95×10^{-14}
40	$O(^1D)+H_2 \rightarrow OH+H$	1.2×10^{-10}
41	$OH+H_2 \rightarrow H_2O+H$	6.67×10^{-15}
42	$NO_2+O(^3p) \rightarrow NO+O_2$	1.03×10^{-11}
43	$NO_2+O(^3p) \rightarrow NO_3$	1.61×10^{-12}
44	$H+NO_2 \rightarrow NO+OH$	1.28×10^{-10}
45	$NO+NO_3 \rightarrow NO_2+NO_2$	2.65×10^{-11}
46	$NO_2+O_3 \rightarrow NO_3+O_2$	3.2×10^{-17}
47	$CO+OH \rightarrow CO_2+H$	2.4×10^{-13}
48	OH deposition/loss	35
49	$CH_3O \rightarrow HCHO+ HO_2$	9.92×10^{3}
50	$CH_3OH+OH \rightarrow HO_2+HCHO$	8.95×10^{-13}
51	$OH+CH_3OOH \rightarrow HCHO+OH$	4.01×10^{-12}
52	$OH+CH_3OOH \rightarrow CH_3O_2$	6.02×10^{-12}
53	$CH_3O_2+CH_3O_2 \rightarrow CH_3OH+HCHO$	4.43×10^{-13}
54	$CH_3O_2+CH_3O_2 \rightarrow CH_3O+CH_3O$	2.58×10^{-13}
55	$CH_3O_2+NO_2 \rightarrow CH_3O_2NO_2$	5.88×10^{-12}
56	$CH_3O_2NO_2 \rightarrow CH_3O_2+NO_2$	1.50
57	$OH+CH_4 \rightarrow CH_3O_2$	6.37×10^{-15}
58	$CH_3O_2+HO_2 \rightarrow CH_3OOH$	4.74×10^{-12}
59	$CH_3O_2+HO_2 \rightarrow HCHO$	4.67×10^{-13}
60	$CH_3O_2+NO \rightarrow CH_3O+NO_2$	7.69×10^{-12}

Table S4. Classification of acetate-CIMS measured species.

Elemental composition	Formula	Assigned category
	DBE=1-3, n_o=2	monoacid
	DBE=2-3, n_o=4	diacid/hydroxycarbonyl acid
No N or S	DBE = 1, n_o = 3−5 or DBE = 2, n_o>4	hydroxy acid
	DBE = 2, n_o = 3 or DBE = 3, $n_o\leq6$	carbonyl acid
	DBE = 5 or 6, n_o = 2−5	aromatic acid
	n_N> 0, and n_S=0	nitrogen (N)-containing compounds (no S)
With N or S	n_S> 0, and n_N=0	sulfur (S)-containing compounds (no N)
	n_N> 0, and n_S>0	N and S-containing compounds

Reference

Ban-Weiss, G. A., Lunden, M. M., Kirchstetter, T. W., and Harley, R. A.: Measurement of black carbon and particle number emission factors from individual heavy-duty trucks, Environmental science & technology, 43, 1419-1424, 2009.

Edwards, R., Mahieu, V., Griesemann, J.-C., Larivé, J.-F., and Rickeard, D. J.: Well-to-wheels analysis of future automotive fuels and powertrains in the European context, SAE Technical Paper0148-7191, 2004.

Gentner, D. R., Jathar, S. H., Gordon, T. D., Bahreini, R., Day, D. A., El Haddad, I., Hayes, P. L., Pieber, S. M., Platt, S. M., de Gouw, J., Goldstein, A. H., Harley, R. A., Jimenez, J. L., Prevot, A. S., and Robinson, A. L.: Review of Urban Secondary Organic Aerosol Formation from Gasoline and Diesel Motor Vehicle Emissions, Environ Sci Technol, 51, 1074-1093, https://doi.org/10.1021/acs.est.6b04509, 2017.

Hak, C. S., Hallquist, M., Ljungstrom, E., Svane, M., and Pettersson, J. B. C.: A new approach to in-situ determination of roadside particle emission factors of individual vehicles under conventional driving conditions, Atmospheric Environment, 43, 2481-2488, 10.1016/j.atmosenv.2009.01.041, 2009.

Hallquist, A. M., Jerksjo, M., Fallgren, H., Westerlund, J., and Sjodin, A.: Particle and gaseous emissions from individual diesel and CNG buses, Atmospheric Chemistry and Physics, 13, 5337-5350, 10.5194/acp-13-5337-2013, 2013.

Lambe, A. T., Ahern, A. T., Williams, L. R., Slowik, J. G., Wong, J. P. S., Abbatt, J. P. D., Brune, W. H., Ng, N. L., Wright, J. P., Croasdale, D. R., Worsnop, D. R., Davidovits, P., and Onasch, T. B.: Characterization of aerosol photooxidation flow reactors: heterogeneous oxidation, secondary organic aerosol formation and cloud condensation nuclei activity measurements, Atmos. Meas. Tech., 4, 445-461, 10.5194/amt-4-445-2011, 2011.

Liu, S., Thompson, S. L., Stark, H., Ziemann, P. J., and Jimenez, J. L.: Gas-phase carboxylic acids in a university classroom: Abundance, variability, and sources, Environmental Science & Technology, 51, 5454-5463, 2017.

Liu, T., Zhou, L., Liu, Q., Lee, B. P., Yao, D., Lu, H., Lyu, X., Guo, H., and Chan, C. K.: Secondary organic aerosol formation from urban roadside air in Hong Kong, Environmental science & technology, 53, 3001-3009, https://doi.org/10.1021/acs.est.8b06587, 2019.

Peng, Z., Day, D. A., Ortega, A. M., Palm, B. B., Hu, W., Stark, H., Li, R., Tsigaridis, K., Brune, W. H., and Jimenez, J. L.: Non-OH chemistry in oxidation flow reactors for the study of atmospheric chemistry systematically examined by modeling, 2016.

Watne, A. K., Psichoudaki, M., Ljungstrom, E., Le Breton, M., Hallquist, M., Jerksjo, M., Fallgren, H., Jutterstrom, S., and Hallquist, A. M.: Fresh and Oxidized Emissions from In-Use Transit Buses Running on Diesel, Biodiesel, and CNG, Environ Sci Technol, 52, 7720-7728, https://doi.org/10.1021/acs.est.8b01394, 2018.

Zhou, L., Hallquist, Å. M., Hallquist, M., Salvador, C. M., Gaita, S. M., Sjödin, Å., Jerksjö, M., Salberg, H., Wängberg, I., and Mellqvist, J.: A transition of atmospheric emissions of particles and gases from on-road heavy-duty trucks, Atmospheric Chemistry and Physics, 20, 1701-1722, 2020.

Zhou, L., Salvador, C. M., Priestley, M., Hallquist, M., Liu, Q., Chan, C. K., and Hallquist, Å. M.: Emissions and secondary formation of air pollutants from modern heavy-duty trucks in real-world traffic—chemical characteristics using on-line mass spectrometry, Environmental Science & Technology, 55, 14515-14525, 2021.